Nanoscale

Cite this: *Nanoscale*, 2012, **4**, 4562

www.rsc.org/nanoscale

PAPER

Generalized syntheses of nanocrystal–graphene hybrids in high-boiling-point organic solvents†

Danny Wei-Ping Pang,‡ Fang-Wei Yuan,‡ Yan-Cheng Chang, Guo-An Li and Hsing-Yu Tuan*

Received 17th April 2012, Accepted 12th May 2012
DOI: 10.1039/c2nr30915g

Nanocrystal–graphene have been proposed as a new kind of promising hybrid for a wide range of application areas including catalysts, electronics, sensors, biomedicine, and energy storage, *etc.* Although a variety of methods have been developed for the preparation of hybrids, a facile and general synthetic approach is still highly required. In this study, nanocrystal–graphene hybrids were successfully synthesized in high-boiling-point organic solvents. Graphene oxide (GO) nanosheets were modified by oleylamine (OLA) to form a OLA–GO complex in order to be readily incorporated into hydrophobic synthesis. A rich library of highly crystalline nanocrystals, with types including noble metal, metal oxide, magnetic material and semiconductor were successfully grown on chemically converted graphene (CCG), which is simultaneously reduced from GO during the synthesis. High boiling-point solvents afford sufficient thermal energy to assure the high-quality crystalline nature of NCs, therefore the post-annealing process is obviated. Controlled experiments revealed that OLA–GO triggers heterogeneous nucleation and serves as excellent nuclei anchorage media. The protocol developed here brings one step closer to achieve "unity in diversity" on the preparation of nanocrystal–graphene hybrids.

Introduction

Graphene, a monolayer graphite and the building block for all other dimensionalities of graphitic materials, has caught immense interest in recent years since Geim and co-workers first isolated it in 2004. Graphene was presumed to never exist in the free 2-dimensional state, which is thermodynamically unstable under finite temperature, but only exists in wrapped-up 0D fullerenes, rolled 1D nanotubes or 3D graphite stacks. Graphene exhibits remarkable electronic, optical, mechanical and thermal properties, *e.g.*, high intrinsic mobility (200 000 $cm^2 v^{-1} s^{-1}$), high fracture strength (~1.0 TPa) and thermal conductivity (~5000 $W m^{-1} K^{-1}$), good chemical stability and high optical transmittance (~98%). In addition, graphene has the largest surface area (2630 $m^2 g^{-1}$) among allotropes of carbon, making it emerging as a promising carbon support for nanocrystals (NCs). The NC–graphene hybrids inherit outstanding mechanical, electronic and thermal properties of graphene synergized with novel optical,[1–5] catalytic, electrical[6] and magnetic[7] properties of inorganic entities,[8–11] making them an exciting class of materials for a variety of application fields such as heterogeneous catalysis, electrochemistry, optical and electro-optical devices, biotechnology applications, and more.[6,12–31]

The most common form of NC–graphene hybrids is based on chemically converted graphene (CCG) as the supportive material. The prevailing synthetic strategies mostly utilize graphene oxide (GO) nanosheets as the starting material for hybrid synthesis, and the method can be summarized by two major categories: *in situ* and *ex situ* growth.[4,24,32–50] In *in situ* growth, NC–CCG hybrids were formed in one-step reactions through various synthetic approaches: solution deposition methods such as reduction of mixed solution,[51–54] microwave heating,[55–57] and sonication-assisted deposition;[5] other growth methods, including polyol reduction,[58] hydrothermal–solvothermal preparation,[45,59,60] and so forth. For instance, Lambert *et al.* prepared titanium oxide–CCG hybrids by hydrolysis of TiF4 in the presence of aqueous graphene oxide solution followed by subsequent thermal reduction.[40,41] Zhu *et al.* prepared NC–CCG hybrids by reduction of metal precursors in metal–ethylene glycol solution of GO.[61] Yang *et al.* pyrolyzed mixture of GO and cobalt phthalocyanine followed by air-oxidation to obtain Co_3O_4–CCG hybrids.[62] On the other hand, in *ex situ* preparation, pre-synthesized NCs are directly assembled on GO or CCG under subsequent treatments such as chemical grafting,[63] layer-by-layer assembly by vacuum filtration,[64] and surfactant interaction.[65] He and Gao functionalized GO with various chemical groups to

Department of Chemical Engineering, National Tsing Hua University, 101, Section 2, Kuang-Fu Road, Hsinchu, Taiwan 30013, ROC. E-mail: hytuan@che.nthu.edu.tw; Fax: +886-3-571-5408; Tel: +886-3-571-5131 ext. 42509

† Electronic supplementary information (ESI) available: detail of experimental parameters, AFM, FTIR, XRD, XPS spectra, and other TEM images of GO, CCG and NC–CCG. See DOI: 10.1039/c2nr30915g

‡ These authors contributed equally to this work.

facilitate the assembly and formation of nanohybrids (Fe_3O_4) and polymer composite (polyurethane).[66] Paek *et al.* reassembled CCG with SnO_2 nanoparticles in ethylene glycol solution.[67] Recently, Lu *et al.* prepared graphene–$Ni(OH)_2$ nanohybrids *via* a mechanically assisted solid-state reaction and showed their improved electrochemical performance as supercapacitor electrode.[16]

The high-temperature colloidal synthesis method, so called hot solvent synthesis, is the most common and probably the most successful method to prepare high quality nanocrystals of diverse kinds with tunable size, shape and composition. High-temperature reactions could effectively decompose organometallic precursors and crystallize NCs in a size- and shape- controllable manner.[68–71] Two techniques are commonly utilized in organic solutions: the "hot-injection" and "heating-up" approaches. The landmark work for "hot-injection" is the cadmium chalcogenide nanocrystals synthesis by Bawendi and co-workers.[71] The idea of this technique is to rapidly inject highly concentrated precursors into "hot-solvent" to facilitate burst nucleation of nanocrystals, followed by the relief of excess free energy of the supersaturation. In heating-up methods, precursors, reagents and solvents are initially mixed together at low temperature and are heated up subsequently to required temperature for initiation of crystallization reaction. This is a batch process which benefits large-scale production and yields high product quality.

In this study, we demonstrate that hot-solvent synthesis is capable of producing NC–CCG hybrids composed of a narrow size distribution of nanocrystals with high-degree of crystallinity *via* a one-step *in situ* growth. NCs, with types covering noble metals, magnetic materials, metal oxides, and binary and ternary semiconductors, could be grown on CCG by the developed method. The properties of as-obtained graphene hybrids were also characterized.

Experimental section

Preparation of GO nanosheets

GO nanosheets were prepared by oxidation and exfoliation of commercially available graphite by Hummers method. 0.5 g of natural graphite (Bay Carbon, SP-1) and 0.5 g of sodium nitrate ($NaNO_3$, J. T. Baker) was mixed in a 500 ml round bottom flask. Concentrated sulfuric acid (95–97%, Sigma-Aldrich) was then added to the mixture under ice bath cooling. Upon reaching 0 °C, 3 g of potassium permanganate ($KMnO_4$, J. T. Baker) was slowly added to the cooled acid solution mixture and the whole pot was transferred to the warm water bath (~40 °C). After stirring for 1 h, the solution was added to 30 ml of deionized (DI) water and left stirring for another 30 min, after which it was further diluted by 100 ml of deionized water. Following the dilution, 3 ml of hydrogen peroxide (30% in water, Sigma-Aldrich) was added dropwise into the solution. The solution was filtered and washed until the filtrate became pH neutral. The filter cake was redispersed in 100 ml DI water and left sonicating for 30 minutes for the exfoliation of graphite oxide. The dispersion was then performed with 8000 rpm centrifugation for 15 minutes, collecting the sediment. The sediment was again redispersed in DI water and 1000 rpm centrifugation was performed for 2 minutes, discarding sediment (note: this step was repeated for 3–5 times until there is no visible particulate). The dispersion was centrifuged with 8000 rpm for 15 minutes to collect the final exfoliated GO product, oven-dried and kept for functionalization and characterization.

Functionalization of GO

5 ml of oleylamine (OLA) (70%, technical grade, Aldrich) and 15 ml of toluene was added to 20 mg of oven-dried GO. Subsequently, the mixture was sonicated for 30 minutes until GO was homogeneously dispersed in the solution, and then the dispersion was centrifuged at 8000 rpm for 15 minutes to collect the sediment. The sediment, referred to as OLA–GO, was redispersed in 40 ml of OLA and kept as stock solution.

Preparation of NC–CCG hybrids

To remove excess OLA before conducting hybrid experiment, 1 ml of OLA–GO (0.5 mg ml^{-1}) stock solution (the quantity used for every hybrid experiment) was added to 20 ml of toluene solution and performed centrifugation at 8000 rpm for 10 minutes. The sediment was redispersed into the solvent used for each hybrid reaction.

The NC–CCG hybrid reactions are categorized into two kinds of experiments: heating-up and hot-injection. For heating-up experiments, the metal precursors and OLA–GO were mixed with organic solvents in a three neck flask connected to the Schlenk line. The whole pot was heated and stirred under elevated temperature for a specific reaction time before the reaction was quenched. The product of NC–CCG hybrids was recovered by repeated centrifugation and washed in the mixture of solvent (toluene) and anti-solvent (ethanol). The final product was redispersed in toluene and kept for further characterization. For hot-injection experiments, similar procedures were carried out except that OLA–GO is dispersed in the injection shot instead of the three neck flask.

Characterization

Height profiles of GO sheets and NC–CCG hybrids were measured on an atomic force microscope (AFM, XE-70, Park System) using the aluminum coating silicon probe (resonant frequency = 300 kHz, force constant = 40 N m^{-1}) under tapping mode with a scanning rate of 1 Hz. TEM images were captured using JEOL-2100F and Philips Technai F20 G2. High resolution X-ray photoelectron spectroscopy (HR-XPS) measurements were performed using PHI Quantera SXM. The Fourier transform infrared (FTIR) spectra were recorded on a Perkin Elmer RXI by the KBr pellet method under transmission mode, acquired from 1000–3750 cm^{-1}, with a resolution of 1 cm^{-1} and 64 scans. X-Ray diffraction (XRD) measurement was carried out using Rigaku Ultima IV at a 2° per min scan rate.

Results and discussion

Scheme 1 illustrates the synthetic procedures. The Hummers method is the most widely used method for the preparation of GO in solution, in which bulk graphite undergoes harsh oxidation to graphite oxide and subsequently exfoliates into single layer graphene oxide (GO). The as-prepared GO is characterized

by atomic force microscopy (AFM) (Fig. S1†). The area of the sample measured is 5 μm × 5 μm, and the height profile is resolved as 0.940 nm, which is consistent with the thickness of a single layer GO sheet. Under TEM observation, GO appeared as a very thin transparent sheet, confirming that exfoliation takes place during sonication. The crumpled silk wave is the landmark of very thin graphene sheet (Fig. S2†). The XRD diffraction pattern for bulk graphite has a very sharp peak at $2\theta = 26.4°$, corresponded to the (002) plane of graphite. When bulk graphite is oxidized into graphite oxide, the diffraction peak at $2\theta = 26.4°$ diminished while a relatively weak and broad peak appeared at $2\theta = 9.8°$. This diffraction peak is assigned to the (001) plane of graphite oxide. This phenomenon is attributed to the expansion of interlayer spacing of graphitic layers when graphite is oxidized into graphite oxide. Graphite oxide is further exfoliated into GO and the diffraction peak at $2\theta = 9.8°$ is diminished, a very small broad diffraction peak appeared at around $2\theta = 20°$ instead, attributed to the disordered GO stacks (Fig. S3†).

GO surface is enriched with oxygen moieties such as epoxy, hydroxyl and edged with carboxyl groups, thus GO is hydrophilic. GO can form well-dispersed suspension since they were highly negatively charged (originated from the ionization of carboxyl and hydroxyl groups) in water, suggesting electrostatic repulsion plays significant role in GO dispersion. These functional groups can be identified by analyzing the sample with FTIR and XPS (Fig. S4 and S5†). The bands located at 1730 cm^{-1} and 1042 cm^{-1} correspond to the C=O and C–O stretching vibrations of the carboxyl group. The band at 1630 cm^{-1} is assigned to the un-oxidized skeletal domain of GO. The broad band at around 3000–3500 cm^{-1} corresponds to the O–H stretching of water molecules adsorbed on the GO surface. The XPS C1s deconvolution spectrum of GO showed three different peaks centered at 284.5 eV, 286.6 eV, and 288 eV, corresponding to C–C/C=C, C–OH and C=O respectively.

However, the hydrophilicity of GO makes it non-dispersible in organic solvents. Without functionalization of OLA, GO sheets readily aggregate in these solvents, hence it would retard the hybrid experiments. We aim to solve this bottleneck by modifying GO surface with a organic surfactant, *i.e.*, oleylamine (OLA), to allow GO to homogeneously disperse in organic solvents. OLA–GO can be readily dispersed in hot-solvents used in our synthetic system, such as toluene, THF, *ortho*-dichlorobenzene, dibenzyl ether, diphenyl ether, *n*-octadecene and tri-octylphosphine. OLA–GO could remain homogeneously dispersed and stable throughout the whole synthetic procedures. The amine-end of OLA was chemically adsorbed on the oxygen moieties of GO with the long hydrophobic chain pointed outward, enabling GO to disperse in organic solvents.[72] Analysis of the FTIR spectrum of OLA–GO provides evidence to the functionalization of GO by oleylamine (OLA) (Fig. S4†). According to the recorded FTIR spectra shown, the bands located at 2850 cm^{-1} and 2925 cm^{-1} in Fig. S4b and S4c† corresponded to anti-symmetric and symmetric C–H stretching vibrations of oleylamine alkyl group respectively. The bands at 1460 cm^{-1} and 1380 cm^{-1} are C–H bending vibrations of alkyl groups. The band 1730 cm^{-1}, which is assigned to –COOH vibrations of GO disappeared after functionalization, and two new bands, 1628 cm^{-1} and 1442 cm^{-1} appeared, as shown in Fig. S4a and S4b†, corresponding to anti-symmetric and symmetric vibrations of COO– respectively, indicating that the carboxyl group is ionized into COO– and confirming the functionalization. As shown in the XPS spectrum (Fig. S5†), remarkable abatement of the epoxy (288.5 eV), and hydroxyl (286.8 eV) groups of OLA–GO compared to GO is attributed to the coupling of OLA on the functional group of GO. The –COOH group of GO ionizes into –COO– and subsequently couples with oleylamine to form a –CO–NH– group.

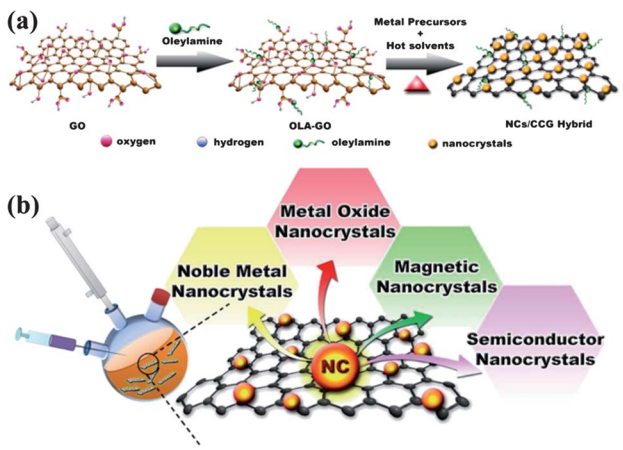

Scheme 1 (a) Synthetic procedure for NC–CCG hybrids by incorporating GO nanosheets into hot-solvent synthesis. (b) Schematic shows that a variety of NC–CCG hybrids could be obtained by the developed approach.

Syntheses of NC–CCG hybrids were carried out in a heating-up or hot-injection ways. NC–CCG hybrids were formed in one-pot reactions by decomposition of metal salts or organometallic precursors in the presence of OLA–GO and synchronously reduced GO to CCG at elevated temperatures in solvents such as *ortho*-dichlorobenzene, *n*-octadecene, benzyl ether and OLA. Detailed experimental parameters are summarized in Table S1†. As shown in Scheme 1b, a rich library of NC–CCG hybrids, including noble metals: Ag, Cu, Pd, Pt, Ru; magnetic materials: Fe_2O_3 and Fe_3O_4; metal oxides: SnO_2, In_2O_3; binary semiconductors: CdS, CdSe, CdTe, ZnS, ZnSe; ternary semiconductors: $CuInS_2$, $CuInSe_2$, on CCG sheets could be obtained by the developed approach. Fig. 1 and Fig. S6† show transmission electron microscopy (TEM) images of as-prepared samples which reveal direct visual observation. The crumpled silk waves in each of the images were attributed to highly exfoliated CCG sheets, mainly consisting of single to a few layers, as confirmed by atomic force microscopy (AFM) characterization. Fig. 2 shows AFM images of the $CuInS_2$–CCG hybrid. The size of $CuInS_2$ nanocrystals is around 5 nm. The corresponding AFM height profile of the hybrid as shown is 12.627 nm, implying that nanocrystals were distributed on both sides of the CCG sheets. However, a minor degree of CCG stacks during the hybrid process could not be ruled out, yet aggregation into thick opaque stacks was apparently absent under TEM observation. In each of the TEM images shown, it is evident that NCs were densely and evenly covered on the surface of CCG, isolated or scattered NCs outside CCG were rarely seen. The NC–CCG hybrids could even withstand intense sonication, repeated washing and

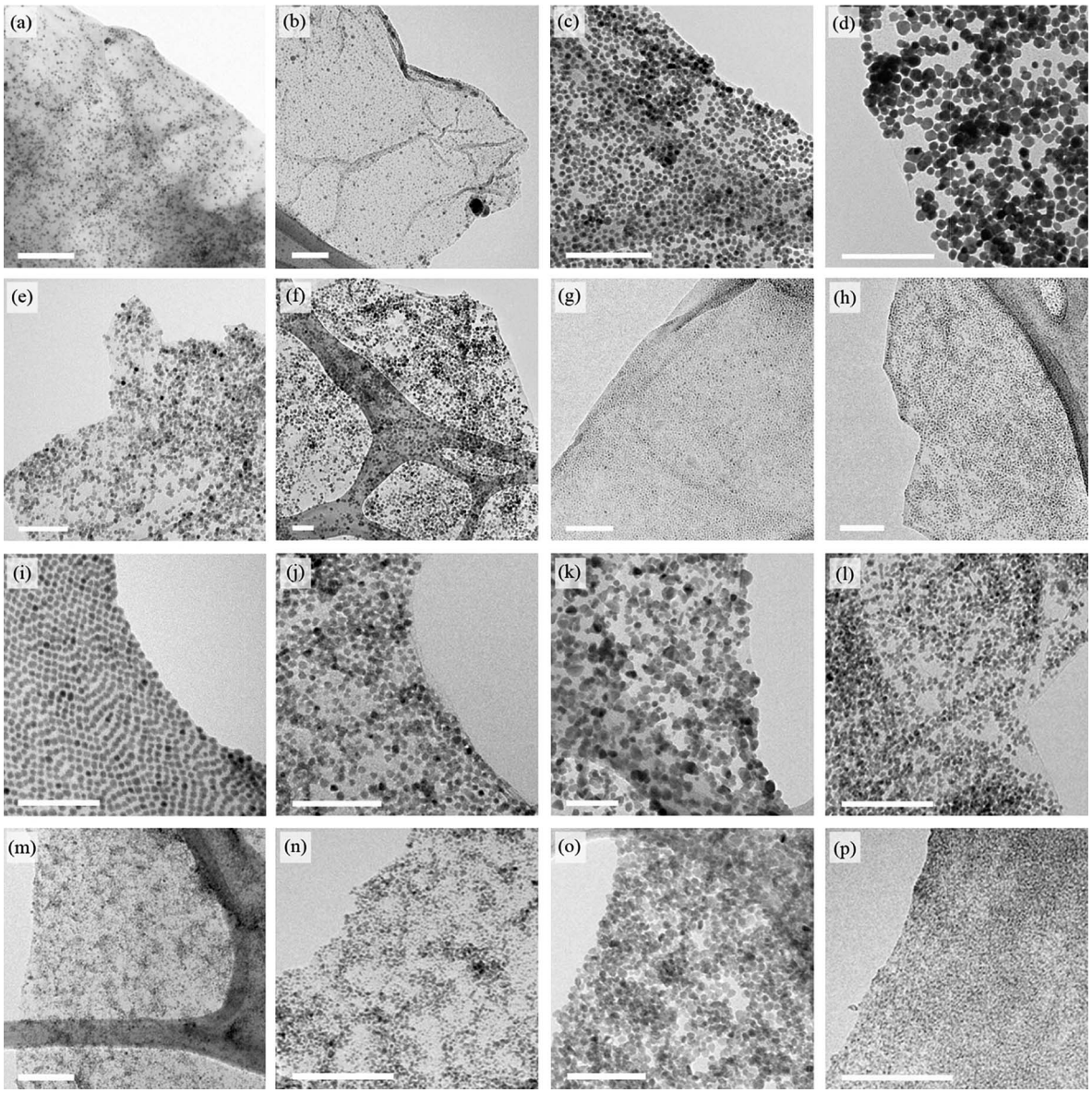

Fig. 1 TEM images of NC–CCG hybrids. NCs include (a) Cu, (b) Ag, (c) Pd, (d) Pt, (e) Fe_3O_4, (f) Fe_2O_3, (g) CdS, (h) CdSe, (i) CdTe, (j) $CuInS_2$, (k) $CuInSe_2$, (l) In_2O_3, (m) SnO_2, (n) Ru, (o) ZnS, (p) ZnSe. Scale bars: 100 nm.

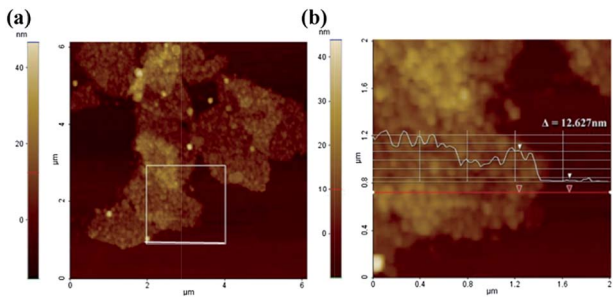

Fig. 2 (a) AFM images of $CuInS_2$–CCG hybrid (area of 6 μm × 6 μm). (b) Height profile of the square cropped-area (2 μm × 2 μm of a). Height difference measured between the hybrid and substrate (the cursor pair in b) is 12.627 nm. The average diameter of $CuInS_2$ nanoparticles is around 5 nm under TEM observation.

centrifugation, showing the NCs tightly bound on the CCG surface. These results validate that the features of these nanoparticles remain intact after hybrid with CCG.

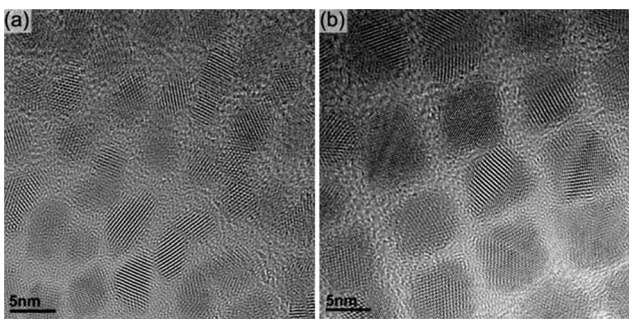

Fig. 3 HRTEM images of (a) CdSe and (b) CdTe NCs on CCG.

High-resolution TEM images revealed the crystalline nature of NCs on CCG. For instance, in the case of CdE (E = S/Se/Te), considerably well-assembled and highly crystalline NCs with a narrow size distribution on CCG were achieved. Such a highly crystalline nature of NCs benefits from achievable high temperature reactions and thus obviates the post-annealing process, greatly simplifying the procedure (Fig. 3). Magnified high-resolution TEM images of all NC–CCG hybrid products (Fig. 4) reveal the single crystalline nature of NCs. The images of individual NCs show clear lattice fringes and highly exposed edges stacked on a CCG. The lattice fringes with different distances were clearly observed, which can be indexed as the specific plane of different NCs. The selected area electron diffraction (SAED) patterns of the NC–CCG hybrid products are shown in Fig. 5, exhibiting sharp diffraction rings corresponding to the specific crystalline planes of the NCs, confirming the formation of crystalline NCs. The HRTEM and SAED patterns also indicate that the NCs attached onto CCG are mainly random orientated.

X-ray diffraction (XRD) patterns (Fig. 6) of all samples are in good agreement with JCPDS database cards as below: Ag (#04-0783), Cu (#04-0836), Pd (#46-1043), Pt (#87-0640), Ru (#06-0663), $CuInS_2$ (#27-0159), $CuInSe_2$ (#40-1487), SnO_2 (#41-1445), In_2O_3 (#06-0416), Fe_2O_3 (#39-1346), Fe_3O_4 (#76-1849), CdS (#01-0647), CdSe (#19-1901), CdTe (#15-770), ZnS (#01-0792), ZnSe (#01-0690). An additional small and broad diffraction peak at around 2θ of 20° (labeled with an asterisk in Fig. 6) in NC–CCG hybrids is attributed to the disordered graphene stacks. We infer that these nanoparticles nucleate on the both sides of the CCG sheets, therefore inhibit the agglomeration of CCG sheets and maintain their high surface area feature.

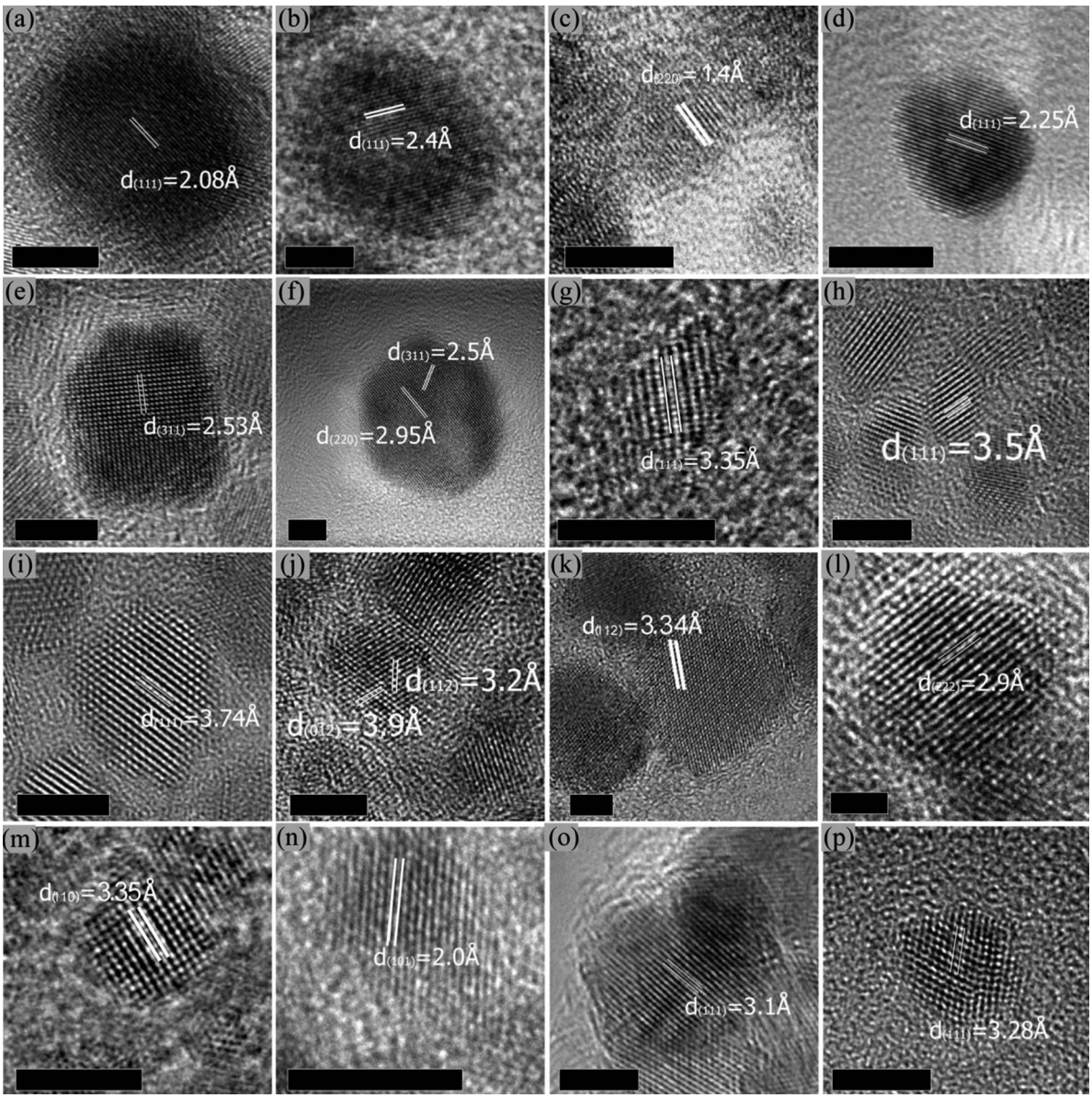

Fig. 4 HRTEM images of NC–CCG hybrids. NCs include (a) Cu, (b) Ag, (c) Pd, (d) Pt, (e) Fe_3O_4, (f) Fe_2O_3, (g) CdS, (h) CdSe, (i) CdTe, (j) $CuInS_2$, (k) $CuInSe_2$, (l) In_2O_3, (m) SnO_2, (n) Ru, (o) ZnS, (p) ZnSe. Scale bars: 5 nm.

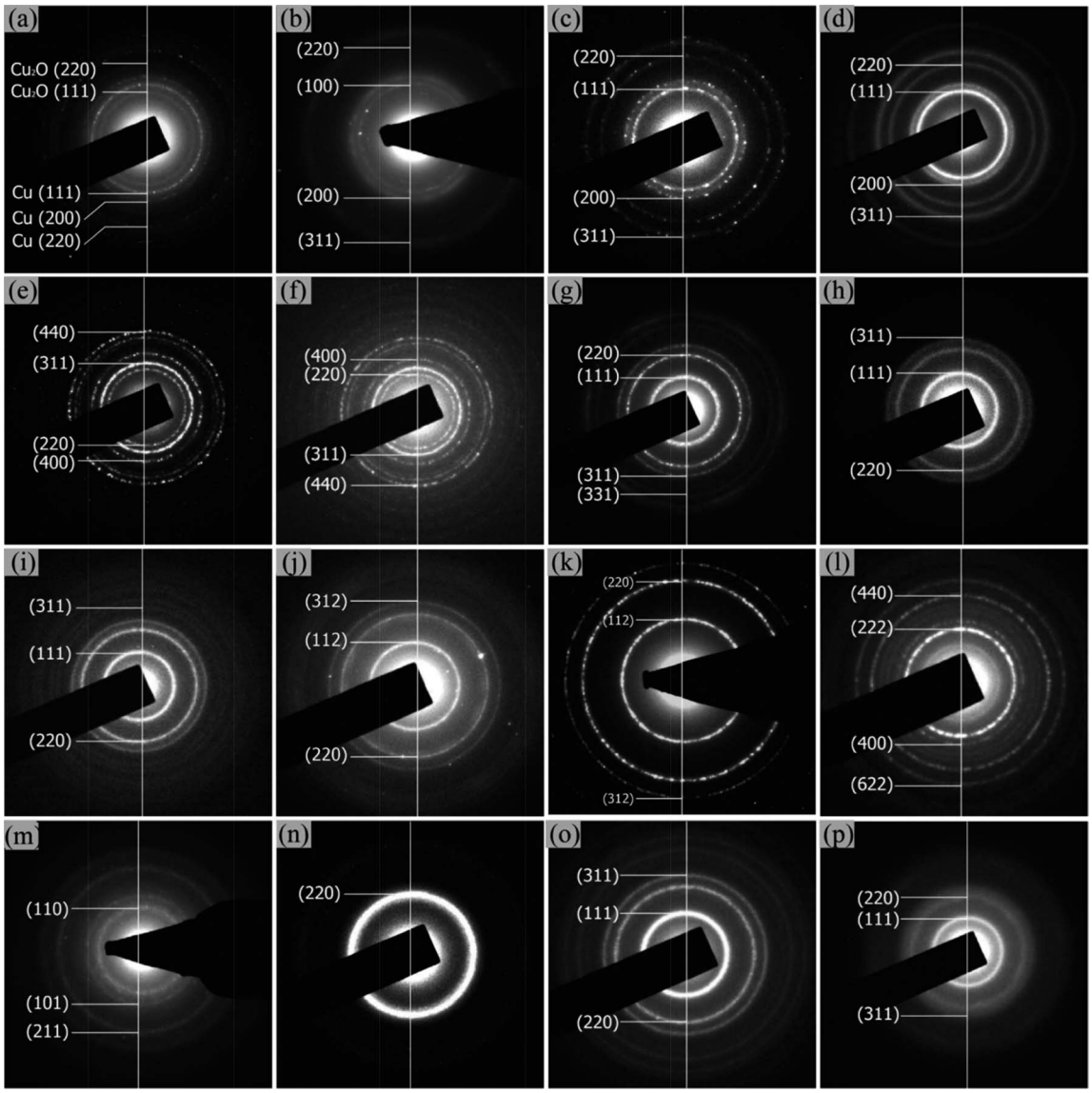

Fig. 5 SAED patterns of NC–CCG hybrids. (a) Cu, (b) Ag, (c) Pd, (d) Pt, (e) Fe_3O_4, (f) Fe_2O_3, (g) CdS, (h) CdSe, (i) CdTe, (j) $CuInS_2$, (k) $CuInSe_2$, (l) In_2O_3, (m) SnO_2, (n) Ru, (o) ZnS, (p) ZnSe.

The chemical conversion of GO to CCG after hybrid formation was confirmed by high-resolution X-ray photoelectron spectroscopy (HR-XPS) of hybrids are shown in Fig. S7†. Deconvolution of the C 1s core level spectra of all NC–CCG hybrids revealed a remarkable abatement of oxygenated peaks (peaks other than 284.6 eV), verified the deoxygenation of GO. The deoxygenation of GO to CCG is likely to arise from amide bonding between oleylamine and oxide functionality which evidently reduced the C–O bonding as observed in XPS analysis. In each of the C 1s core level spectra shown below, it is evident that there is a deconvoluted peak appeared in 285.2 eV. This peak is originally absent from GO, we proposed that during hybrid syntheses, the condensation reaction might as well take place forming an amide bond. Previous study also found similar reactions when hydrazine monohydrate was used to reduce GO to CCG.[73]

Pt–CCG hybrid synthesis was investigated as a representative case to account for the formation mechanism. We used the exact same experiment conditions except without the addition of OLA–GO. Severe aggregates of Pt NCs can be observed in Fig. 7a. Compared with the one with OLA–GO added, Pt NCs were uniformly dispersed on CCG (Fig. 7b) and there were no large clusters as appeared in Fig. 7a. XRD characterization was carried out for these two samples. A strong and narrow peak was observed in the sample without OLA–GO, whereas a slightly broader and weaker peak was observed with the Pt–CCG hybrids. A strong narrow peak is normally observed when the nanocrystals are highly crystalline or appear in the form of a large cluster. On the contrary, in the sample with OLA–GO added, a slightly weaker peak was observed, this is likely due to well dispersed and relatively small size of nanoparticles (Fig. S8†). Such striking differences in the Pt NCs' morphologies

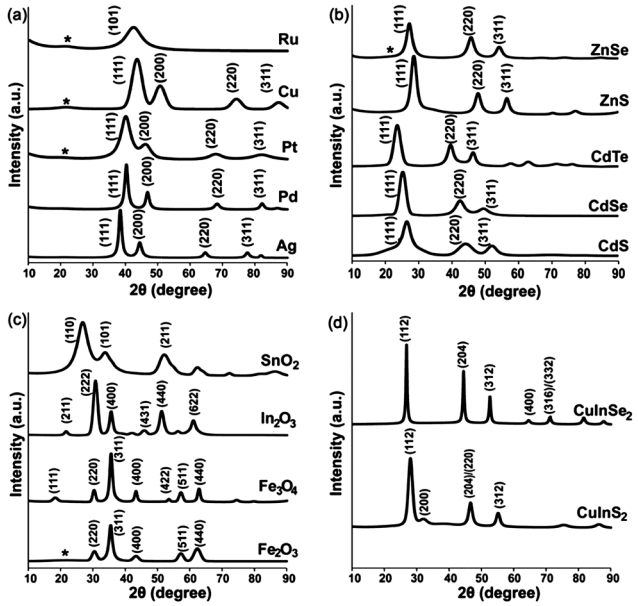

Fig. 6 XRD patterns of NC–CCG hybrids. (a) Noble metals which include Ag, Pd, Pt, Cu, Ru; (b) binary semiconductors: CdS, CdSe, CdTe, ZnS, ZnSe; (c) magnetic and metal oxides: Fe_2O_3, Fe_3O_4, In_2O_3, SnO_2; (d) ternary semiconductors: $CuInS_2$ and $CuInSe_2$.

demonstrates that OLA–GO indeed plays a significant role in supporting and mediating the growth of nanoparticles.

The large basal plane of CCG sheets provides many excellent nucleation sites for the nucleation of NCs. It is generally accepted that the surface energy of newly formed nuclei is very high and unstable that they tend to homogeneously interact with neighboring nuclei to form NCs and clusters or heterogeneously interact with surface present in the solution to lower its surface energy. In terms of Gibbs free energy, heterogeneous nucleation has a much lower energy barrier (ΔG^*_{hetero}) to surpass than the activation energy barrier (ΔG^*_{homo}) of homogeneous nucleation to create new crystal embryos, *i.e.*, $\Delta G^*_{hetero} = f(\theta)\ \Delta G^*_{homo}$, where $f(\theta)$ is the wetting function; since newly generated monomers possess very high surface energy, the presence of heterogeneity in the solution therefore triggered heterogeneous nucleation of monomers which were more thermodynamically favorable.[74] Previous studies reported that GO sheet is enriched with hydroxyl and epoxy groups on its basal planes while carboxyl groups located at its edge.[75] These functional groups were found to be responsible to act as anchor sites for nucleation and promote interaction with nanoparticles.[52] Based on the fundamental insights presented above, the formation mechanism of NC–CCG hybrids in our approach is put forward. Monomers were generated by thermal decomposition of organometallic precursors at a designated temperature. Homogeneous dispersion of GO in reaction media exposed their large surface area to reactants and effectively facilitated the heterogeneous nucleation of NCs. The abundance of functional groups on the basal planes and edges of GO served as excellent nucleation sites to accommodate nuclei and sustain further growth and crystallization of nanoparticles.

The properties of graphene hybrids were characterized. SnO_2–CCG hybrids obtained from this were used as the anode

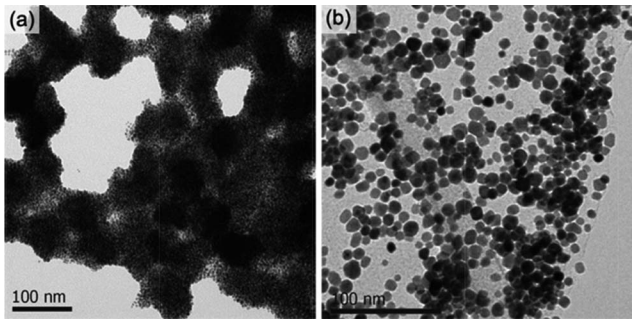

Fig. 7 TEM images of Pt nanocrystals synthesized from reactions (a) without and (b) with the addition of OLA–GO.

of lithium-ion battery and showed good retention of reversible capacity with a coulombic efficiency of >96% for the hybrids, which indicates a good charge–discharge performance (Fig. 8). The stability is probably because the CCG layers act as an "elastic" buffer layer to the expansion of nanocrystals, inhibiting the damage caused during Li^+ intercalation.[67] The initial specific capacity for the half-cell battery was 510 mA h g^{-1} and the capacity remained at 470 mA h g^{-1} after 20 cycles. The Pt–CCG hybrid showed remarkable activity for the catalytic potential on methanol oxidation, which is commonly applied in direct methanol fuel cells (DMFCs) (Fig. 8). Supported nanosized Pt on large surface area CCG stabilized the catalytic particles at the same time exposing great electrochemical surface area, therefore enhancing the overall methanol oxidation performance.[76] The methanol oxidation peak appeared at 0.7 V while oxidation peak of residual carbon species appeared at 0.5 V. Fe_3O_4–CCG hybrids exhibit superparamagnetic behaviour with no coercivity and remanence (Fig. 8), consistent with the theory of ferromagnetic to superparamagnetic conversion when the particle size is smaller than 25 nm under superconducting quantum interference device (SQUID) test. These hybrids show reasonable composite characteristics and are potential materials for a wide range of applications.

Conclusions

In summary, we have demonstrated that "unity in diversity" for the synthesis of NC–CCG hybrids might be attainable by incorporating surface-modified GO into the existing hot-solvent methods. Oleylamine-functionalized GO gives ready access to the hydrophobic synthetic systems and facilitates heterogeneous nucleation of NCs. Compared with other approaches, our synthetic protocol ensures high-quality NCs on graphene sheets with high reproducibility thanks to the synthetic capability of hot-solvent systems. Furthermore, a better understanding of kinetics and thermodynamics of this approach will provide profound insight to master and rationally tailor the NCs' chemical composition (*e.g.*, alloying and doping), size and shape, and complex architectures (*e.g.*, core–shell and heterostructures) on graphene sheets,[77–83] thus be able to create more versatile NC–graphene hybrids for many fundamental discoveries and technological applications.

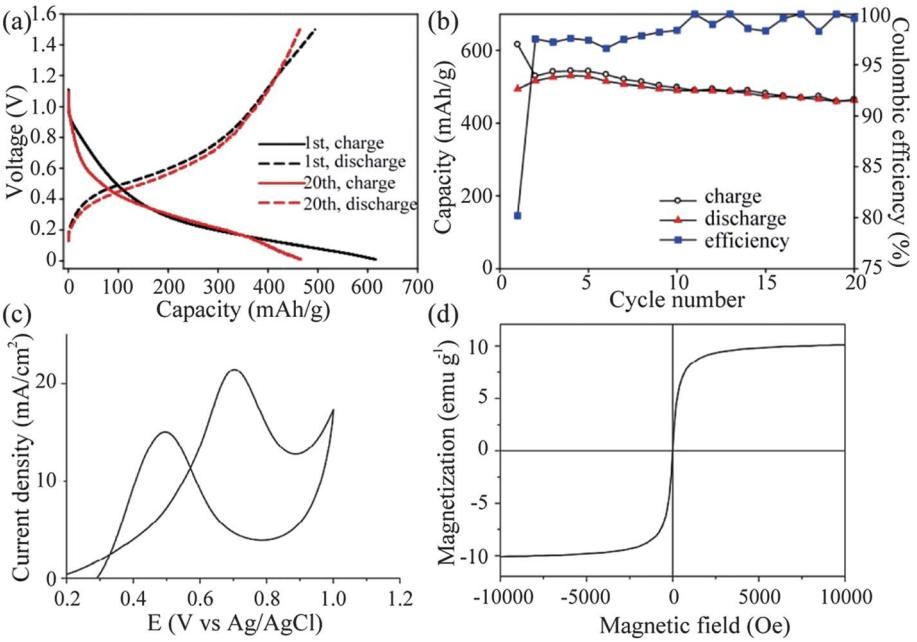

Fig. 8 (a) 1st and 20th charge–discharge profiles, (b) cyclic performance of SnO_2–CCG hybrid, (c) linear sweep voltammogram of Pt–CCG hybrid on glassy carbon electrode, carried out in a solution of 0.5 M H_2SO_4 with 1 M methanol at a 0.05 V s^{-1} scan rate, (d) magnetization curve of Fe_2O_3–CCG hybrid at 300 K.

Acknowledgements

The authors acknowledge the financial support by the National Science Council of Taiwan (NSC 99-2221-E-007-096, NSC 100-3113-E-007-008, NSC 100-2628-E-007-029-MY2), National Tsing Hua University (100N2060E1, 100N2041E1), the Ministry of Economic Affairs (101-EC-17-A-09-S1-198), and the HRTEM (JEOL JEM-2100F) assistance from Tamkang University College of Science.

Notes and references

1 C. N. R. Rao, A. K. Sood, K. S. Subrahmanyam and A. Govindaraj, *Angew. Chem., Int. Ed.*, 2009, **48**, 7752.
2 D. R. Dreyer, R. S. Ruoff and C. W. Bielawski, *Angew. Chem., Int. Ed.*, 2010, **49**, 9336.
3 K. S. Novoselov, A. K. Geim, S. V. Morozov, D. Jiang, Y. Zhang, S. V. Dubonos, I. V. Grigorieva and A. A. Firsov, *Science*, 2004, **306**, 666.
4 G. Williams and P. V. Kamat, *Langmuir*, 2009, **25**, 13869.
5 K. Vinodgopal, B. Neppolian, I. V. Lightcap, F. Grieser, M. Ashokkumar and P. V. Kamat, *J. Phys. Chem. Lett.*, 2010, **1**, 1987.
6 J. Yang, C. G. Tian, L. Wang and H. G. Fu, *J. Mater. Chem.*, 2011, **21**, 3384.
7 S. X. Wu, Z. Y. Yin, Q. Y. He, G. Lu, X. Z. Zhou and H. Zhang, *J. Mater. Chem.*, 2011, **21**, 3467.
8 X. M. Lu, M. Rycenga, S. E. Skrabalak, B. Wiley and Y. N. Xia, *Annu. Rev. Phys. Chem.*, 2009, **60**, 167.
9 Y. Xu, N. Al-Salim, C. W. Bumby and R. D. Tilley, *J. Am. Chem. Soc.*, 2009, **131**, 15990.
10 W. Wei, S. Z. Li, L. D. Qin, C. Xue, J. E. Millstone, X. Y. Xu, G. C. Schatz and C. A. Mirkin, *Nano Lett.*, 2008, **8**, 3446.
11 Y. N. Xia, Y. J. Xiong, B. Lim and S. E. Skrabalak, *Angew. Chem., Int. Ed.*, 2009, **48**, 60.
12 S. Moussa, A. R. Siamaki, B. F. Gupton and M. S. El-Shall, *ACS Catal.*, 2012, **2**, 145.
13 L. L. Li, K. P. Liu, G. H. Yang, C. M. Wang, J. R. Zhang and J. J. Zhu, *Adv. Funct. Mater.*, 2011, **21**, 869.
14 Y. Lin, K. Zhang, W. F. Chen, Y. D. Liu, Z. G. Geng, J. Zeng, N. Pan, L. F. Yan, X. P. Wang and J. G. Hou, *ACS Nano*, 2010, **4**, 3033.
15 G. Y. Chen, D. W. P. Pang, S. M. Hwang, H. Y. Tuan and Y. C. Hu, *Biomaterials*, 2012, **33**, 418.
16 Z. Sun and X. Lu, *Ind. Eng. Chem. Res.*, 2012, DOI: 10.1021/ie202706h.
17 H. Zhao, J. Yang, L. Wang, C. G. Tian, B. J. Jiang and H. G. Fu, *Chem. Commun.*, 2011, **47**, 2014.
18 H. Hayashi, I. V. Lightcap, M. Tsujimoto, M. Takano, T. Umeyama, P. V. Kamat and H. Imahori, *J. Am. Chem. Soc.*, 2011, **133**, 7684.
19 J. X. Zhu, T. Zhu, X. Z. Zhou, Y. Y. Zhang, X. W. Lou, X. D. Chen, H. Zhang, H. H. Hng and Q. Y. Yan, *Nanoscale*, 2011, **3**, 1084.
20 J. X. Zhu, Z. Y. Lu, M. O. Oo, H. H. Hng, J. Ma, H. Zhang and Q. Y. Yan, *J. Mater. Chem.*, 2011, **21**, 12770.
21 J. X. Zhu, K. Sun, D. H. Sim, C. Xu, H. Zhang, H. H. Hng and Q. Yan, *Chem. Commun.*, 2011, **47**, 10383.
22 C. X. Peng, B. D. Chen, Y. Qin, S. H. Yang, C. Z. Li, Y. H. Zuo, S. Y. Liu and J. H. Yang, *ACS Nano*, 2012, **6**, 1074.
23 S. B. Yang, X. L. Feng and K. Mullen, *Adv. Mater.*, 2011, **23**, 3575.
24 S. B. Yang, X. L. Feng, S. Ivanovici and K. Mullen, *Angew. Chem., Int. Ed.*, 2010, **49**, 8408.
25 L. Kavan, J. H. Yum, M. K. Nazeeruddin and M. Gratzel, *ACS Nano*, 2011, **5**, 9171.
26 G. H. Yu, L. B. Hu, N. A. Liu, H. L. Wang, M. Vosgueritchian, Y. Yang, Y. Cui and Z. A. Bao, *Nano Lett.*, 2011, **11**, 4438.
27 X. Zhao, C. M. Hayner, M. C. Kung and H. H. Kung, *Adv. Energy Mater.*, 2011, **1**, 1079.
28 K. Jagannadham, *J. Appl. Phys.*, 2011, **110**, 094907.
29 J. Yang, S. Y. Deng, J. P. Lei, H. X. Ju and S. Gunasekaran, *Biosens. Bioelectron.*, 2011, **29**, 159.
30 J. S. Zhou, L. L. Ma, H. H. Song, B. Wu and X. H. Chen, *Electrochem. Commun.*, 2011, **13**, 1357.
31 X. Sun, M. Xie, G. K. Wang, H. T. Sun, A. S. Cavanagh, J. J. Travis, S. M. George and J. Lian, *J. Electrochem. Soc.*, 2012, **159**, A364.
32 I. V. Lightcap, T. H. Kosel and P. V. Kamat, *Nano Lett.*, 2010, **10**, 577.
33 M. R. Das, R. K. Sarma, R. Saikia, V. S. Kale, M. V. Shelke and P. Sengupta, *Colloids Surf., B*, 2011, **83**, 16.
34 S. B. Yang, X. L. Feng, L. Wang, K. Tang, J. Maier and K. Mullen, *Angew. Chem., Int. Ed.*, 2010, **49**, 4795.

35 J. B. Liu, S. H. Fu, B. Yuan, Y. L. Li and Z. X. Deng, *J. Am. Chem. Soc.*, 2010, **132**, 7279.
36 B. F. Machado and P. Serp, *Catal. Sci. Technol.*, 2012, **2**, 54.
37 S. X. Wu, Z. Y. Yin, Q. Y. He, G. Lu, Q. Y. Yan and H. Zhang, *J. Phys. Chem. C*, 2011, **115**, 15973.
38 S. Moussa, V. Abdelsayed and M. S. El-Shall, *Chem. Phys. Lett.*, 2011, **510**, 179.
39 S. Bai and X. P. Shen, *Prog. Chem.*, 2010, **22**, 2106.
40 T. N. Lambert, C. A. Chavez, B. Hernandez-Sanchez, P. Lu, N. S. Bell, A. Ambrosini, T. Friedman, T. J. Boyle, D. R. Wheeler and D. L. Huber, *J. Phys. Chem. C*, 2009, **113**, 19812.
41 T. N. Lambert, C. A. Chavez, N. S. Bell, C. M. Washburn, D. R. Wheeler and M. T. Brumbach, *Nanoscale*, 2011, **3**, 188.
42 D. H. Wang, R. Kou, D. Choi, Z. G. Yang, Z. M. Nie, J. Li, L. V. Saraf, D. H. Hu, J. G. Zhang, G. L. Graff, J. Liu, M. A. Pope and I. A. Aksay, *ACS Nano*, 2010, **4**, 1587.
43 G. Williams, B. Seger and P. V. Kamat, *ACS Nano*, 2008, **2**, 1487.
44 K. Jasuja, J. Linn, S. Melton and V. Berry, *J. Phys. Chem. Lett.*, 2010, **1**, 1853.
45 H. L. Wang, L. F. Cui, Y. A. Yang, H. S. Casalongue, J. T. Robinson, Y. Y. Liang, Y. Cui and H. J. Dai, *J. Am. Chem. Soc.*, 2010, **132**, 13978.
46 H. L. Wang, J. T. Robinson, G. Diankov and H. J. Dai, *J. Am. Chem. Soc.*, 2010, **132**, 3270.
47 Z. S. Wu, W. C. Ren, L. Wen, L. B. Gao, J. P. Zhao, Z. P. Chen, G. M. Zhou, F. Li and H. M. Cheng, *ACS Nano*, 2010, **4**, 3187.
48 S. F. Bartolucci, J. Paras, M. A. Rafiee, J. Rafiee, S. Lee, D. Kapoor and N. Koratkar, *Mater. Sci. Eng., A*, 2011, **528**, 7933.
49 W. He, H. J. Jiang, Y. Zhou, S. D. Yang, X. Z. Xue, Z. Q. Zou, X. G. Zhang, D. L. Akins and H. Yang, *Carbon*, 2012, **50**, 265.
50 W. Qian, Z. Q. Chen, S. Cottingham, W. A. Merrill, N. A. Swartz, A. M. Goforth, T. L. Clare and J. Jiao, *Green Chem.*, 2012, **14**, 371.
51 J. T. Zhang, Z. G. Xiong and X. S. Zhao, *J. Mater. Chem.*, 2011, **21**, 3634.
52 C. Xu, X. Wang, J. W. Zhu, X. J. Yang and L. Lu, *J. Mater. Chem.*, 2008, **18**, 5625.
53 G. X. Wang, B. Wang, X. L. Wang, J. Park, S. X. Dou, H. Ahn and K. Kim, *J. Mater. Chem.*, 2009, **19**, 8378.
54 X. Z. Tang, Z. W. Cao, H. B. Zhang, J. Liu and Z. Z. Yu, *Chem. Commun.*, 2011, **47**, 3084.
55 P. Kundu, C. Nethravathi, P. A. Deshpande, M. Rajamathi, G. Madras and N. Ravishankar, *Chem. Mater.*, 2011, **23**, 2772.
56 H. M. A. Hassan, V. Abdelsayed, A. E. R. S. Khder, K. M. AbouZeid, J. Terner, M. S. El-Shall, S. I. Al-Resayes and A. A. El-Azhary, *J. Mater. Chem.*, 2009, **19**, 3832.
57 A. F. Zedan, S. Sappal, S. Moussa and M. S. El-Shall, *J. Phys. Chem. C*, 2010, **114**, 19920.
58 J. F. Shen, M. Shi, N. Li, B. Yan, H. W. Ma, Y. Z. Hu and M. X. Ye, *Nano Res.*, 2010, **3**, 339.
59 X. D. Huang, X. F. Zhou, L. A. Zhou, K. Qian, Y. H. Wang, Z. P. Liu and C. Z. Yu, *ChemPhysChem*, 2011, **12**, 278.
60 W. H. Shi, J. X. Zhu, D. H. Sim, Y. Y. Tay, Z. Y. Lu, X. J. Zhang, Y. Sharma, M. Srinivasan, H. Zhang, H. H. Hng and Q. Y. Yan, *J. Mater. Chem.*, 2011, **21**, 3422.
61 C. Xu, X. Wang and J. W. Zhu, *J. Phys. Chem. C*, 2008, **112**, 19841.
62 S. B. Yang, G. L. Cui, S. P. Pang, Q. Cao, U. Kolb, X. L. Feng, J. Maier and K. Mullen, *ChemSusChem*, 2010, **3**, 236.
63 F. A. He, J. T. Fan, D. Ma, L. M. Zhang, C. Leung and H. L. Chan, *Carbon*, 2010, **48**, 3139.
64 B. S. Kong, J. X. Geng and H. T. Jung, *Chem. Commun.*, 2009, 2174.
65 X. M. Geng, L. Niu, Z. Y. Xing, R. S. Song, G. T. Liu, M. T. Sun, G. S. Cheng, H. J. Zhong, Z. H. Liu, Z. J. Zhang, L. F. Sun, H. X. Xu, L. Lu and L. W. Liu, *Adv. Mater.*, 2010, **22**, 638.
66 H. K. He and C. Gao, *Chem. Mater.*, 2010, **22**, 5054.
67 S. M. Paek, E. Yoo and I. Honma, *Nano Lett.*, 2009, **9**, 72.
68 J. Park, J. Joo, S. G. Kwon, Y. Jang and T. Hyeon, *Angew. Chem., Int. Ed.*, 2007, **46**, 4630.
69 X. G. Peng, L. Manna, W. D. Yang, J. Wickham, E. Scher, A. Kadavanich and A. P. Alivisatos, *Nature*, 2000, **404**, 59.
70 D. Kim, N. Lee, M. Park, B. H. Kim, K. An and T. Hyeon, *J. Am. Chem. Soc.*, 2009, **131**, 454.
71 C. B. Murray, D. J. Norris and M. G. Bawendi, *J. Am. Chem. Soc.*, 1993, **115**, 8706.
72 Y. Matsuo, T. Miyabe, T. Fukutsuka and Y. Sugie, *Carbon*, 2007, **45**, 1005.
73 S. Stankovich, D. A. Dikin, R. D. Piner, K. A. Kohlhaas, A. Kleinhammes, Y. Jia, Y. Wu, S. T. Nguyen and R. S. Ruoff, *Carbon*, 2007, **45**, 1558.
74 L. Carbone and P. D. Cozzoli, *Nano Today*, 2010, **5**, 449.
75 T. Szabo, O. Berkesi, P. Forgo, K. Josepovits, Y. Sanakis, D. Petridis and I. Dekany, *Chem. Mater.*, 2006, **18**, 2740.
76 Y. M. Li, L. H. Tang and J. H. Li, *Electrochem. Commun.*, 2009, **11**, 846.
77 S. Cheong, J. Watt, B. Ingham, M. F. Toney and R. D. Tilley, *J. Am. Chem. Soc.*, 2009, **131**, 14590.
78 F. Shieh, A. E. Saunders and B. A. Korgel, *J. Phys. Chem. B*, 2005, **109**, 8538.
79 T. T. Toan and X. M. Lu, *J. Phys. Chem. C*, 2011, **115**, 3638.
80 Y. W. Jun, J. S. Choi and J. Cheon, *Angew. Chem., Int. Ed.*, 2006, **45**, 3414.
81 Q. A. Zhang, W. Y. Li, C. Moran, J. Zeng, J. Y. Chen, L. P. Wen and Y. N. Xia, *J. Am. Chem. Soc.*, 2010, **132**, 11372.
82 S. H. Choi, H. B. Na, Y. I. Park, K. An, S. G. Kwon, Y. Jang, M. Park, J. Moon, J. S. Son, I. C. Song, W. K. Moon and T. Hyeon, *J. Am. Chem. Soc.*, 2008, **130**, 15573.
83 Y. Ding, F. R. Fan, Z. Q. Tian and Z. L. Wang, *J. Am. Chem. Soc.*, 2010, **132**, 12480.

